



**HAL**  
open science

## Corrosion inhibition of copper in 0.5 M NaCl solutions by aqueous and hydrolysis acid extracts of olive leaf

Philippe Refait, Chahla Rahal, Mohamed Masmoudi

► **To cite this version:**

Philippe Refait, Chahla Rahal, Mohamed Masmoudi. Corrosion inhibition of copper in 0.5 M NaCl solutions by aqueous and hydrolysis acid extracts of olive leaf. *Journal of Electroanalytical Chemistry*, 2020, 859, pp.113834. 10.1016/j.jelechem.2020.113834 . hal-02473288

**HAL Id: hal-02473288**

**<https://univ-rochelle.hal.science/hal-02473288>**

Submitted on 21 Jul 2022

**HAL** is a multi-disciplinary open access archive for the deposit and dissemination of scientific research documents, whether they are published or not. The documents may come from teaching and research institutions in France or abroad, or from public or private research centers.

L'archive ouverte pluridisciplinaire **HAL**, est destinée au dépôt et à la diffusion de documents scientifiques de niveau recherche, publiés ou non, émanant des établissements d'enseignement et de recherche français ou étrangers, des laboratoires publics ou privés.



Distributed under a Creative Commons Attribution - NonCommercial 4.0 International License

1 **Timing of oocyte recruitment within the ovulatory cycle of Macedonian**  
2 **shad, *Alosa macedonica*, a batch spawning fish with indeterminate**  
3 **fecundity**

4  
5 Foivos Alexandros Mouchlianitis<sup>a</sup>, George Minos<sup>b</sup>, Kostas Gantias<sup>a</sup>

6  
7 <sup>a</sup>School of Biology, Aristotle University of Thessaloniki, Thessaloniki, Greece

8 <sup>b</sup>School of Health Sciences, Department of Nursing, International Hellenic University,  
9 Thessaloniki, Greece

10

11 Correspondence: F. A. Mouchlianitis; School of Biology, Aristotle University of Thessaloniki,  
12 Thessaloniki, Greece; Email: amouchl@bio.auth.gr; ORCID: 0000-0003-3050-0877

13

14 **Abstract**

15 The recruitment of primary growth (PG) oocytes to the secondary growth (SG) phase within  
16 the ovulatory cycle, i.e. time interval between two sequential ovulation/spawning events, has  
17 rarely been examined in detail in a quantitative manner for batch spawning fishes with  
18 indeterminate fecundity. In the present study we analyzed the ovarian dynamics of  
19 Macedonian shad, *Alosa macedonica*, an iteroparous batch spawning clupeid with  
20 indeterminate fecundity, with the main goal to define the timing of PG recruitment and relate  
21 it to the ovulatory cycle. The latter was classified into four different phases (pre-ovulatory,  
22 running, post-ovulatory, intermediate) through postovulatory follicles and presence/absence  
23 of hydrated oocytes. Various indices of ovarian dynamics, including the formation and mean  
24 diameter of the advanced oocyte batch, the ovarian developmental stage, the oocyte size  
25 modality and the gonadosomatic index, varied among the ovulatory phases, evidencing  
26 cyclicity. Relative fecundity of newly recruited SG oocytes was used as an index of PG  
27 recruitment intensity and was shown to follow a specific pattern within the ovulatory cycle;  
28 PG recruitment occurred in a stepwise manner and in parallel with ovulation of the advanced

29 oocyte batch, and synchronization of these two processes kept the ovary in a state of dynamic  
30 equilibrium.

31

## 32 **Keywords**

33 Batch spawning, indeterminate fecundity, ovarian dynamics, oocyte recruitment, ovulation  
34 cyclicality

35

## 36 **1. Introduction**

37 Many fish species are classified as batch (or multiple, partial, serial, heterochronal; [1,2])  
38 spawners, since they release their oocytes in multiple events within a spawning season [3-5].

39 Thus, during the ovulatory cycle, i.e. time interval between two sequential  
40 ovulation/spawning events, of a batch spawner, ovarian developmental processes take place  
41 so the first event will be followed by the second, the second by the third, and so on. In case  
42 of batch spawners with determinate fecundity type, these ovarian processes pertain mainly  
43 to the secondary growth phase (SG) and the development of the advanced batch to be  
44 spawned next [6]. On the contrary, in batch spawners exhibiting indeterminate fecundity type,  
45 the ovarian processes that occur within the ovulatory cycle include both the formation of the  
46 advanced oocyte batch and the recruitment of oocytes from the primary (PG) to the SG phase  
47 (i.e. PG recruitment) [6].

48 The development of the advanced oocyte batch can follow different patterns among fishes  
49 [7] and has been studied extensively in both determinate (e.g. [6,8]) and indeterminate (e.g.  
50 [9-12]) spawners. The process of PG recruitment has also been examined both qualitatively  
51 (e.g. [13-15]) and quantitatively (e.g. [16-21]). During the last decade, significant progress has  
52 been made in terms of small-sized oocyte characterization and quantification, mainly by the  
53 development of the oocyte packing density theory (OPD) [22], which led to advanced and very  
54 detailed distinction of small-sized PG and SG oocytes into developmental stages and  
55 estimation of their numbers in each of these stages [17-20]. In specific, Korta et al. (2010)  
56 combined advanced OPD, stereological techniques and the auto-diametric method [23] to  
57 examine the early cycle oocyte recruitment dynamics in European hake, *Merluccius merluccius*  
58 [17]. Kjesbu et al. (2011) established the “grid method”, which is a simpler version of OPD, to  
59 quantify PG and SG oocyte production in Atlantic cod, *Gadus morhua*, [18]. OPD was also

60 implemented to study the ovarian dynamics of the European anchovy, *Engraulis encrasicolus*  
61 [19]. Moreover, Serrat et al. (2019) analyzed the seasonal ovarian dynamics in European hake  
62 via advanced OPD [20]. Most of these studies were focused on broad temporal scales, such as  
63 the reproductive season or the spawning season. To our knowledge, only the paper of  
64 Schismenou et al. (2012) provided suggestions regarding the underlying mechanisms of PG  
65 recruitment within the narrow temporal scale of the ovulatory cycle [19]. In specific, the latter  
66 study suggested recruitment “in rapid pulses of less than 24-h (possibly few hours) activated  
67 by the hydration of the spawning batch” in European anchovy.

68 To fill this gap, we analyzed the ovarian dynamics of Macedonian shad, *Alosa macedonica*, an  
69 iteroparous batch spawning clupeid with indeterminate fecundity [24, authors unpublished  
70 data], within the ovulatory cycle, with the main goal to define the timing of PG recruitment  
71 and relate it to ovulation cyclicity. To do so, the ovulatory cycle was classified into four  
72 different phases. Ovarian developmental indices were compared among these phases to  
73 assess ovulation cyclicity in the best detail possible and to define the timing of PG recruitment.  
74 This study analyzed both the formation of the advanced oocyte batch and PG recruitment  
75 within the ovulatory cycle and intended to find a temporal association between these two  
76 ovarian processes.

77

## 78 **2. Materials and methods**

79 Fish were collected with vertical gill nets during the night on five sampling dates in June 2016  
80 (Table 1), i.e. during the spawning season [24]. All fish were immediately stored in 10% neutral  
81 buffered formalin. The biometric measurements included total length (in mm), total weight  
82 (in g), eviscerated weight ( $W_{ev}$  in g) and gonad weight ( $W_g$  in g). Gonadosomatic index was also  
83 estimated ( $GSI = 100 \times W_g/W_{ev}$ ).

84 Ovarian subsamples from 91 mature females were processed histologically (~2mm thick hand-  
85 cut cross sections, paraffin embedding, 4- $\mu$ m sections, hematoxylin/eosin staining) and  
86 through whole-mount procedure (Table 1). Each histological section was digitized into a high-  
87 resolution photomicrograph using a BASLER acA1920-40uc camera fitted on a Zeiss Axio  
88 Lab.A1 microscope and the Microvisioneer software, and each whole-mount subsample was  
89 digitally imaged using a Jenoptik Progress C3 camera mounted on a Euromex NZ 80 stereo  
90 microscope. Prior to digitalization, whole-mount subsamples were stained with hematoxylin  
91 to increase oocyte opacity and prevent possible overlook due to their original transparency.

92 The photomicrographs enabled, for each female: (i) identification of the distinct oocyte  
93 developmental stages at both the PG and the SG phase, (ii) detection of postovulatory follicles  
94 (POF), measurement of the cross-sectional area of the biggest POF in the section,  $POF_{XSA}$  (see  
95 [25]), and classification of each  $POF_{XSA}$  as large or small based on its histomorphological  
96 characteristics [26,27] and its value, and (iii) definition of the ovarian developmental stage as  
97 the stage of the most advanced oocytes in the histological section. We identified: cortical  
98 alveolar (CA) oocyte stages, three vitellogenic (VIT-1 – VIT-3) stages, the germinal vesicle  
99 migration (GVM) stage and the hydration (HYD) stage [28].

100 Whole-mount photos were analyzed through the auto-diametric method and particle analysis  
101 [23] to estimate oocyte sizes and to create the oocyte size frequency distributions (OSFDs).  
102 Each OSFD was subsequently analyzed through the Bhattacharya method [29] to identify any  
103 clearly distinguished modes and to estimate the size (i.e. number of oocytes) and the mean  
104 oocyte diameter (OD) of each mode, as has been previously done for Allis shad, *A. alosa* [21]  
105 and Alewife *A. pseudoharengus* [30]. The advanced mode (AM) was separated in all OSFDs  
106 (see Results section) and consequently, its relative fecundity (i.e. number of oocytes per g of  
107  $W_{ev}$ ) was estimated through the gravimetric method [2] using the formula:

$$108 \quad RF_{AM} = \frac{n_{AM} \times \frac{W_g}{W_{SS}}}{W_{ev}}$$

109 where  $n_{AM}$  was the number of oocytes of the AM and  $W_{SS}$  the weight of the whole-mount  
110 subsample. AM corresponded to the spawning batch, i.e. to the oocytes that are released  
111 during a single spawning episode, and thus  $RF_{AM}$  was equivalent to relative batch fecundity  
112 (number of oocytes released per spawning event per g of  $W_{ev}$ ;  $RF_b$ ). To avoid possible bias,  $RF_b$   
113 was estimated only from hydrated females prior to an ovulation event, i.e. those classified as  
114 in pre-ovulatory phase (see Results section).

115 To estimate relative total fecundity (i.e. number of all SG oocytes per g of  $W_{ev}$ ;  $RF_t$ ), we set the  
116 size threshold between PG and SG oocytes at 200  $\mu$ m, based on previous values reported for  
117 Allis shad [21] and American shad *A. sapidissima* [31].  $RF_t$  was estimated gravimetrically for  
118 each female by using the formula:

$$119 \quad RF_t = \frac{n_t \times \frac{W_g}{W_{SS}}}{W_{ev}}$$

120 where  $n_t$  was the number of all SG oocytes of the whole-mount subsample.

121 Recruitment intensity was assessed through the relative fecundity of the small-sized SG  
122 oocytes, i.e. those with diameter between 200 and 320  $\mu\text{m}$  ( $\text{RF}_{200-320}$ ), based on previously  
123 implemented methodology [16]. The ratio of  $\text{RF}_t$  to mean  $\text{RF}_b$  of females at the pre-ovulatory  
124 phase (fecundity ratio) was used as a proxy of the number of co-occurring SG oocyte batches,  
125 as has been done in previous study [12]. In females caught while ovulating, (running; see  
126 Results section), the fecundity ratio was estimated by subtracting the remaining hydrated  
127 oocytes from  $\text{RF}_t$  and adding unity to the resulting  $\text{RF}_t/\text{RF}_b$  quotient to counterbalance the  
128 missing ovulating batch.

129 Cyclicity was examined by comparing the numerical formation of the AM and the mean  
130 diameter of the AM ( $\text{OD}_{\text{AM}}$ ), the ovarian developmental stage, the modality of OSFDs and GSI  
131 among the different ovulatory phases (see Results section).

132 We used R 3.5.2 [32] to perform the statistical analyses and to create the plots. The specific R  
133 packages used in this study were: *ggplot2*, *ggridges*, *ggpubr* [33-35]. Normality was tested by  
134 the Shapiro test.

135

### 136 **3. Results**

#### 137 *3.1 Ovulatory phases classification*

138 Multiple SG oocyte developmental stages were present in each ovary. All females were  
139 spawning capable (i.e. with oocytes at an advanced stage, capable of spawning during the  
140 current reproductive period; [28]). High proportion of females (87%) had POF in their ovaries.  
141 Most of these ovaries (82.5%) had POF from two different cohorts (new and old), which  
142 originated from two sequential daily spawning events (Fig. 1). Thus, POF degeneration period  
143 was constantly longer than the ovulatory cycle.  $\text{POF}_{\text{XSA}}$  of the newest cohort in each ovary,  
144 classified as large, had values  $> 0.05 \text{ mm}^2$ , while small  $\text{POF}_{\text{XSA}}$  had values  $< 0.02 \text{ mm}^2$  (Fig. 2).

145 Four phases were identified within the ovulatory cycle based on the presence/absence of HYD  
146 oocytes and the presence of large or small  $\text{POF}_{\text{XSA}}$  (Table 2): (1) pre-ovulatory (PRE), (2) running  
147 (RUN), (3) post-ovulatory (POST), and (4) intermediate (INT). The criterion of  $\text{POF}_{\text{XSA}}$  of the  
148 newest cohort was clear-cut, especially for distinguishing PRE from RUN and POST from INT  
149 females (Fig. 3). The few females without POF in their ovaries had HYD oocytes and were  
150 classified as PRE.

151

152 *3.2 Ovarian dynamics cyclicity*

153 The profiles of AM formation, as overviewed in Figure 4, revealed that AM was discernible in  
154 all four ovulatory phases. However, there were clear differences; the AM was gradually  
155 becoming completely separated from the smaller oocytes as ovulatory cycle progressed from  
156 POST to RUN females (Fig. 4). Cyclicity was evinced also through the ovarian developmental  
157 stage; both PRE and RUN females were at the HYD stage, POST females were at the VIT-2 or  
158 VIT-3 stage, and all INT females had progressed to VIT-3 or GVM ovarian stage (Fig. 4).

159 Detailed analysis of OSFDs revealed co-occurrence of various distinct modes within the  
160 smaller oocytes (SM1, SM2, etc.) (Fig. 5). In general, as females were approaching an ovulation  
161 event (PRE females), the different modes were becoming more distinct (Fig. 5).

162 GSI and mean  $OD_{AM}$  also exhibited a clear pattern, evidencing the continuity of ovarian  
163 dynamics within the ovulatory cycle (Fig. 6). Prior to an ovulation event (PRE females), GSI and  
164  $OD_{AM}$  were at their maximum values (mean GSI  $\pm$  SD =  $21.6 \pm 3.3$ ; mean  $OD_{AM} \pm$  SD =  $864 \pm 36$   
165  $\mu\text{m}$ ). Subsequently, both GSI and  $OD_{AM}$  followed a decreasing trend and dropped to their  
166 minimum values (mean GSI  $\pm$  SD =  $8.6 \pm 2.3$ ; mean  $OD_{AM} \pm$  SD =  $500 \pm 33 \mu\text{m}$ ) in POST females.  
167 As females approached readiness to ovulate again (INT females), both GSI and  $OD_{AM}$  increased  
168 (mean GSI  $\pm$  SD =  $9.5 \pm 1.5$ ; mean  $OD_{AM} \pm$  SD =  $604 \pm 50 \mu\text{m}$ ). Mean GSI and  $OD_{AM}$  values were  
169 significantly different from one ovulatory phase to the next (least significant difference, 95%  
170 confidence level,  $P < 0.05$ ). The only two exceptions were the lack of statistically significant  
171 difference in GSI between POST and INT females and in  $OD_{AM}$  between PRE and RUN females  
172 (least significant difference, 95% confidence level,  $P > 0.05$ ).

173

174 *3.3 Timing of PG Recruitment*

175 PG recruitment occurred stepwise and in parallel with the ovulation of the advanced oocyte  
176 batch. RUN females had higher mean ( $\pm$  SD)  $RF_{200-320}$  values ( $411 \pm 162$  oocytes per g)  
177 compared to PRE ( $323 \pm 118$  oocytes per g) and INT ( $270 \pm 99$  oocytes per g) females (least  
178 significant difference, 95% confidence level,  $P < 0.05$ ; Fig. 7a). In addition, RUN females had  
179 higher mean ( $\pm$  SD) fecundity ratio ( $3.5 \pm 0.9$ ) than PRE ( $2.9 \pm 0.6$ ), POST ( $2.3 \pm 0.8$ ) and INT ( $2$   
180  $\pm 0.4$ ) females (least significant difference, 95% confidence level,  $P < 0.05$ ; Fig. 7b). The mean  
181  $RF_b$  of PRE females used to estimate the fecundity ratio values was 415 oocytes per g.

182

## 183 4. Discussion

184 Batch spawning fishes with either determinate or indeterminate fecundity display ovulation  
185 cyclicity, i.e. processes occur within the ovulatory cycle to accomplish egg release in multiple  
186 sequential events during their spawning period. The ovarian processes that take place within  
187 the ovulatory cycle in indeterminate batch spawners include mainly the formation of the  
188 advanced oocyte batch to be spawned next and the recruitment of oocytes from the primary  
189 (PG) to the secondary (SG) growth phase (PG recruitment). The formation of the advanced  
190 batch has been frequently analyzed, whilst the PG recruitment has often been overlooked and  
191 rarely examined in detail and in a quantitative manner at the fine temporal scale of the  
192 ovulatory cycle. In this study, we evinced cyclicity and we analyzed both the formation of the  
193 advanced batch and PG recruitment within the ovulatory cycle in an indeterminate batch  
194 spawning fish, Macedonian shad *A. macedonica*. Our results enabled the detection of the  
195 timing of PG recruitment within the ovulatory cycle and revealed a temporal association  
196 between ovulation of the advanced oocyte batch and PG recruitment.

197 Ovulation cyclicity in batch spawning fishes has been demonstrated in different ways, such as  
198 behavioral observations [36,37] and analyses of hormone profiles [38-40]. Especially, cyclicity  
199 in ovarian processes has been evinced through different indices and in many species [9-  
200 12,38,41]. In case of *A. macedonica*, we showed that ovarian processes were occurring within  
201 the ovulatory cycle by comparing several indices among four different ovulatory phases: the  
202 AM numerical formation and the  $OD_{AM}$ , the ovarian developmental stage, the modality of  
203 OSFDs and GSI. All these indices displayed specific patterns within the ovulatory cycle, and  
204 thus evinced the continuity of ovarian dynamics between sequential ovulation events. GSI and  
205  $OD_{AM}$  followed an increasing trend from the completion of an ovulation event and prior to the  
206 next. The modality of OSFDs was getting more obvious and the AM was becoming more  
207 separated from the smaller oocytes as females were approaching an ovulation event. In  
208 addition, the developmental stage of the AM was more advanced in females that were prior  
209 to an ovulation event than in those that had just ovulated.

210 The two main ovarian processes that take place within the ovulatory cycle of indeterminate  
211 batch spawners have been analyzed disproportionately. The formation of the advanced  
212 oocyte batch has been analyzed extensively (e.g. [9-12,38,41,42]), whilst detailed analyses of  
213 PG recruitment have been conducted at a far less extent. The studies focused on PG  
214 recruitment were either qualitative, resulting in detailed description of the sequential  
215 developmental oocyte stages prior and after the recruitment process [15,43,44], or

216 quantitative [16, 18-20]. Most of these latter studies used advanced quantification techniques  
217 to analyze PG recruitment process mostly during broad temporal scales, such as the  
218 reproductive season and the spawning season [18-20], or rarely during the narrower temporal  
219 scale of the ovulatory cycle [19]. In this study, we implemented the auto-diametric method  
220 [23] with a few modifications (hematoxylin staining to increase PG and small SG oocyte  
221 opacity), which may be less informative regarding the stages of oocytes but has been proven  
222 effective in quantifying small-sized oocytes (e.g. [21,45]).

223 Comparisons in recruitment intensity and fecundity ratio among females at different  
224 ovulatory phases revealed a clear pattern of PG recruitment. Females caught during ovulation  
225 had higher recruitment intensity and fecundity ratio compared to females at earlier or later  
226 ovulatory phases, revealing that a new batch of SG oocytes was recruited from the pool of PG  
227 reserves at a specific time-frame, during the ovulation of the advanced oocyte batch. Our  
228 conclusion is corroborated by previous reports for another indeterminate batch spawning  
229 clupeid, European anchovy [19]. More specifically, the latter study suggested that oocyte  
230 recruitment occurred in swift pulses triggered by the hydration of the spawning batch.

231 Figure 8 depicts a conceptual model of the ovarian dynamics within the ovulatory cycle in an  
232 indeterminate batch spawner. In summary, PG recruitment and ovulation of the advanced  
233 batch are synchronized, keeping the ovary in a state of a dynamic equilibrium regarding  $RF_t$   
234 and number of SG batches in the ovary, while GSI and  $OD_{AM}$  fluctuate between relatively  
235 constant minimum and maximum values. The concept of a dynamic equilibrium in the ovaries  
236 of actively spawning indeterminate batch spawners has been previously suggested. Mature  
237 ovaries of Northern anchovy *E. mordax* were shown to contain a stable number of oocyte  
238 batches; result attributed to the theoretically continuous recruitment of small oocytes in  
239 parallel with spawning activity [46]. Additionally, model simulations suggested that PG  
240 recruitment kept pace with spawning of the advanced oocyte batch, and thus sustained a  
241 balanced number of oocyte batches and total fecundity in indeterminate batch spawners [47].  
242 Finally, detailed analysis, through the OPD [22], suggested that oocyte numbers in the ovaries  
243 were in a steady state, displaying an equilibrium, also in European anchovy [19]. Our study  
244 evinced the concept of dynamic equilibrium within the ovulatory cycle and reported a  
245 temporal association between ovulation of the advanced oocyte batch and PG recruitment.  
246 The described association did not provide any justification of a cause-effect relationship  
247 between the two ovarian processes and we suggest this matter to be analyzed in future  
248 studies.

249

## 250 **Acknowledgements**

251 The authors are grateful to A. Alexiadou for assisting the biometric measurements and the  
252 preparation of whole-mount subsamples and histological sections. The research work was  
253 supported by the Hellenic Foundation for Research and Innovation (HFRI) and the General  
254 Secretariat for Research and Technology (GSRT), under the HFRI PhD Fellowship grant  
255 attributed to F.A. Mouchlianitis (GA. No. 493584).

256

## 257 **Declarations of interest**

258 Declarations of interest: none

259

## 260 **Table titles**

261 **Table 1.** Number (N) of females analyzed histologically and through whole-mount analysis,  
262 and total length (in mm) range, mean and standard deviation (S.D.), per sampling date

263 **Table 2.** Phases identified within the ovulatory cycle, based on the presence/absence (+/-) of  
264 hydrated (HYD) oocytes, presence/absence (+/-) of postovulatory follicles (POF) and cross-  
265 sectional area of the biggest POF (POF<sub>XSA</sub>).

266

## 267 **Figure captions**

268 **Figure 1.** Photomicrograph of an ovarian histological section (hematoxylin/eosin staining)  
269 showing postovulatory follicles (POF) from two different ovulation events (old and new POF  
270 cohorts).

271 **Figure 2.** Frequency distribution of the cross-sectional area (in mm<sup>2</sup>) of the biggest  
272 postovulatory follicle (POF<sub>XSA</sub>) in each of the 79 ovaries analyzed. Two POF<sub>XSA</sub> size classes were  
273 distinguished: small (area < 0.02 mm<sup>2</sup>) and large (area > 0.05 mm<sup>2</sup>).

274 **Figure 3.** Violin plot of the cross-sectional area (in mm<sup>2</sup>) of the biggest postovulatory follicle  
275 (POF<sub>XSA</sub>) in each ovarian histological section for females at different phases within the  
276 ovulatory cycle: prior to an ovulation event (pre-ovulatory phase), during ovulation (running

277 phase), immediately or closely after an ovulation (post-ovulatory phase) and in-between two  
278 ovulation events (intermediate phase). Colors and shapes represent the ovarian  
279 developmental stages, i.e. the stage of the most advanced oocytes in each ovary. VIT-2 =  
280 secondary vitellogenic stage, VIT-3 = tertiary vitellogenic stage, GVM = germinal vesicle  
281 migration stage, HYD = hydration stage.

282 **Figure 4.** Size frequency distributions of oocytes at the secondary growth phase for females  
283 at different phases within the ovulatory cycle: prior to an ovulation event (pre-ovulatory  
284 phase), during ovulation (running phase), immediately or closely after an ovulation (post-  
285 ovulatory phase) and in-between two ovulation events (intermediate phase). Color of each  
286 distribution represents the ovarian developmental stage, i.e. the stage of the most advanced  
287 oocytes in the ovary. Within each panel, distributions are displayed in order of increasing  
288 (bottom to top) mean oocyte diameter of the secondary growth oocytes. VIT-2 = secondary  
289 vitellogenic stage, VIT-3 = tertiary vitellogenic stage, GVM = germinal vesicle migration stage,  
290 HYD = hydration stage.

291 **Figure 5.** Size frequency distributions of oocytes at the secondary growth phase and the  
292 corresponding ovarian histological sections for females at different phases within the  
293 ovulatory cycle: (a–b) immediately or closely after an ovulation (post-ovulatory phase; POST),  
294 (c–d) in-between two ovulation events (intermediate phase; INT), and (e–f) prior to an  
295 ovulation event (pre-ovulatory phase; PRE). AM = advanced mode, SM1 = first subsequent  
296 mode, SM2 = second subsequent mode, SM3 = third subsequent mode, PG = primary growth  
297 stage, CA = cortical alveolar stages, VIT-1 = primary vitellogenic stage, VIT-2 = secondary  
298 vitellogenic stage, VIT-3 = tertiary vitellogenic stage, HYD = hydration stage, POF =  
299 postovulatory follicle.

300 **Figure 6.** Line plot of mean values and confidence intervals of: (a) gonadosomatic index (GSI)  
301 and (b) diameter (in  $\mu\text{m}$ ) of the advanced oocyte batch ( $\text{OD}_{\text{AM}}$ ), for females at different phases  
302 within the ovulatory cycle: prior to an ovulation event (pre-ovulatory phase), during ovulation  
303 (running phase), immediately or closely after an ovulation (post-ovulatory phase) and in-  
304 between two ovulation events (intermediate phase). Statistically significant pairwise  
305 comparisons of mean values are shown with asterisks (“\*\*\*” for  $P < 0.01$ , “\*\*\*\*” for  $P < 0.001$ ).

306 **Figure 7.** Line plot of mean values and confidence intervals of: (a) relative fecundity of small  
307 oocytes at the secondary growth phase, i.e. with diameter between 200 and 320  $\mu\text{m}$  (Relative  
308 fecundity<sub>200-320</sub>), and (b) fecundity ratio (total fecundity/batch fecundity), for females at  
309 different phases within the ovulatory cycle: prior to an ovulation event (pre-ovulatory phase),

310 during ovulation (running phase), immediately or closely after an ovulation (post-ovulatory  
311 phase) and in-between two ovulation events (intermediate phase). Statistically significant  
312 pairwise comparisons of mean values are shown with asterisks (“\*” for P < 0.05, “\*\*\*\*” for P <  
313 0.001).

314 **Figure 8.** Conceptual model of the ovarian dynamics within the ovulatory cycle in an  
315 indeterminate batch spawning fish. Prior to an ovulation event (pre-ovulatory phase),  
316 gonadosomatic index (GSI) and diameter of the most advanced oocytes (OD<sub>AM</sub>) are at their  
317 maximum values and any postovulatory follicles (POF) present originated from a previous  
318 ovulation (old POF cohort), are already partially absorbed, and thus have small area. In parallel  
319 with ovulation of the advanced batch (running phase), a new oocyte batch is recruited from  
320 the primary growth to the secondary growth phase (PG recruitment), resulting in an oocyte  
321 size frequency distribution (OSFD) with an additional mode. Concurrently, GSI begins to  
322 decrease and old POF continue to shrink, while a new POF cohort is forming. Immediately or  
323 closely after the ovulation (post-ovulatory phase), the OSFD is comprised by several  
324 overlapping modes, GSI drops to its lowest values, old POF continue to decrease in size and  
325 new POF start to degenerate. As females approach readiness to ovulate again (intermediate  
326 phase), the advanced mode becomes gradually separated in the OSFD, GSI and OD<sub>AM</sub> start to  
327 elevate again and old POF absorption is likely complete, while new POF degeneration  
328 continues. The OSFDs in the lower panel are “snapshots” of the secondary growth phase of  
329 the ovarian development for the different phases within the ovulatory cycle.

330

## 331 **References**

332 [1] Holden MJ, Raitt DFS. Manual of Fisheries Science. Part 2: Methods of resource  
333 investigation and their application. FAO Fish Tech Rep 1974;115 (rev. 1), Rome, Italy.

334 [2] Hunter JR, Lo NCH, Leong RJH. Batch fecundity in multiple spawning fishes. In: Lasker R,  
335 editor. An Egg Production Method for Estimating Spawning Biomass of Pelagic Fish:  
336 Application to the Northern Anchovy, *Engraulis mordax*. NOAA Techn Rep NMFS; 1985;36,  
337 p. 67–77.

338 [3] McEvoy LA, McEvoy J. Multiple spawning in several commercial fish species and its  
339 consequences for fisheries management, cultivation and experimentation. J Fish Biol  
340 1992;41:125–36. doi:10.1111/j.1095-8649.1992.tb03874.x

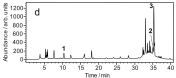
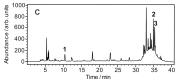
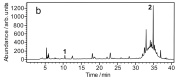
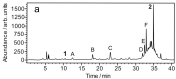
341 [4] Lowerre-Barbieri SK, Lowerre JM, Barbieri LR. Multiple spawning and dynamics of fish  
342 populations: inferences from an individual-based simulation model. Can J Fish Aquat Sci  
343 1998;55:2244–54.

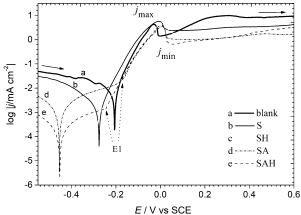
- 344 [5] Murua H, Saborido-Rey F. Female reproductive strategies of marine fish species of the  
345 North Atlantic. *J Northw Atl Fish Sci* 2003;33:23–31.
- 346 [6] Hunter JR, Macewicz BJ, Lo NCH, Kimbrell CA. Fecundity, spawning, and maturity of female  
347 Dover sole *Microstomus pacificus*, with an evaluation of assumptions and precision. *Fish*  
348 *Bull* 1992;90:101–28.
- 349 [7] Wallace RA, Selman K. Cellular and dynamic aspects of oocyte growth in teleosts. *Amer*  
350 *Zool* 1981;21:325–43.
- 351 [8] Kjesbu OS, Witthames PR, Solemdal P, Greer-Walker M. Ovulatory rhythm and a method  
352 to determine the stage of spawning in Atlantic cod (*Gadus morhua*). *Can J Fish Aquat Sci*  
353 1990;47(6):1185–93.
- 354 [9] Ganas K, Somarakis S, Machias A, Theodorou A. Pattern of oocyte development and batch  
355 fecundity in the Mediterranean sardine. *Fish Res* 2004;67:13–23.
- 356 [10] Murua H, Motos L. Reproductive strategy and spawning activity of the European hake  
357 *Merluccius merluccius* (L.) in the Bay of Biscay. *J Fish Biol* 2006;69(5):1288–303.  
358 doi:10.1111/j.1095-8649.2006.01169.x
- 359 [11] Ferreri R, Ganas K, Genovese S, Fontana I, Giacalone G, Bonanno A, Mazzola S et al.  
360 Oocyte batch development and enumeration in the European anchovy (*Engraulis*  
361 *encrasicolus*). *Mediterr Mar Sci* 2016;17(3):670–7. doi: 10.12681/mms.1693.
- 362 [12] Ganas K, Mouchlianitis FA, Nunes C, Costa AM, Angélico MM. A reassessment of the  
363 fecundity type of Atlantic horse mackerel (*Trachurus trachurus*) in Atlantic Iberian waters  
364 (ICES division IXa) shows that indeterminate spawners can cease recruiting oocytes  
365 during their spawning season. *ICES J Mar Sci* 2017;74(1):31–40.
- 366 [13] Selman K, Wallace RA. Cellular aspects of oocyte growth in teleosts. *Zool Sci* 1989;6:211–  
367 31.
- 368 [14] Grier HJ, Uribe MC, Patiño R. The ovary, folliculogenesis, and oogenesis in teleosts. In:  
369 Jamieson BGM, editor. *Reproductive Biology and Phylogeny of Fishes (Agnathans and*  
370 *Bony Fishes)*, Vol. 8A. Science Publishers, Enfield, New Hampshire; 2009; p. 25–84.
- 371 [15] Uribe MC, Grier HJ, García-Alarcón A, Parenti LR. Oogenesis: From oogonia to ovulation  
372 in the flagfish, *Jordanella floridae* Goode and Bean, 1879 (Teleostei: Cyprinodontidae). *J*  
373 *Morphol* 2016;277(10):1339–54.
- 374 [16] Greer-Walker M, Witthames PR, Bautista de los Santos I. Is the fecundity of the Atlantic  
375 Mackerel (*Scomber scombrus*: Scombridae) determinate? *Sarsia* 1994;79:13–26.
- 376 [17] Korta M, Murua H, Kurita Y, Kjesbu OS. How are the oocytes recruited in an indeterminate  
377 fish? Applications of stereological techniques along with advanced packing density theory  
378 on European hake (*Merluccius merluccius* L.). *Fish Res* 2010;104:56–63.
- 379 [18] Kjesbu OS, Thorsen A, Fonn M. Quantification of primary and secondary oocyte  
380 production in Atlantic cod by simple oocyte packing density theory. *Mar Coast Fish*  
381 2011;3:92–105. doi: 10.1080/19425120.2011.555714

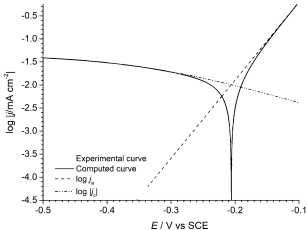
- 382 [19] Schismenou E, Somarakis S, Thorsen A, Kjesbu OS. Dynamics of de novo vitellogenesis in  
383 fish with indeterminate fecundity: an application of oocyte packing density theory to  
384 European anchovy, *Engraulis encrasicolus*. Mar Biol 2012;159:757–68.
- 385 [20] Serrat A, Saborido-Rey F, Garcia-Fernandez C, Muñoz M, Lloret J, Thorsen A, Kjesbu OS.  
386 New insights in oocyte dynamics shed light on the complexities associated with fish  
387 reproductive strategies. Sci Rep 2019;9:18411. doi:10.1038/s41598-019-54672-3
- 388 [21] Mouchlianitis FA, Belo AF, Vieira AR, Quintella BR, Almeida PR, Ganas K. Primary and  
389 secondary oocyte growth dynamics in anadromous semelparous Allis shad *Alosa alosa*. J  
390 Fish Biol 2019;95:1447–56. doi:10.1111/jfb.14161
- 391 [22] Kurita Y, Kjesbu OS. Fecundity estimation by oocyte packing density formulae in  
392 determinate and indeterminate spawners: Theoretical considerations and applications.  
393 J Sea Res 2009;61:188–96. doi: 10.1016/j.seares.2008.10.010
- 394 [23] Thorsen A, Kjesbu OS. A rapid method for estimation of oocyte size and potential  
395 fecundity in Atlantic cod using a computer-aided particle analysis system. J Sea Res  
396 2001;46:295–308.
- 397 [24] Kleanthidis PK. Biology of the reproduction, feeding habits and population dynamics of  
398 the endemic fish *Alosa macedonica* (Vinciguerra, 1921) of Lake Volvi. Doctoral  
399 Dissertation, 2002, Aristotle University of Thessaloniki (in Greek).
- 400 [25] Ganas K, Nunes C, Stratoudakis Y. Degeneration of postovulatory follicles in the Iberian  
401 sardine *Sardina pilchardus*: structural changes and factors affecting resorption. Fish Bull  
402 2007;105:131–9.
- 403 [26] Hunter JR, Goldberg SR. Spawning incidence and batch fecundity in northern anchovy,  
404 *Engraulis mordax*. Fish Bull 1980;77:641–52.
- 405 [27] Hunter JR Macewicz BJ. Measurements of spawning frequency in multiple spawning  
406 fishes. In: Lasker R, editor. An Egg Production Method for Estimating Spawning Biomass  
407 of Pelagic Fish: Application to the Northern Anchovy, *Engraulis mordax*. NOAA Techn Rep  
408 NMFS; 1985;36, p. 79–84.
- 409 [28] Brown-Peterson NJ, Wyanski DM, Saborido-Rey F, Macewicz BJ, Lowerre-Barbieri SK. A  
410 standardized terminology for describing reproductive development in fishes. Mar Coast  
411 Fish 2011;3:52–70. doi: 10.1080/19425120.2011.555724
- 412 [29] Bhattacharya CG A simple method of resolution of a distribution into Gaussian  
413 components. Biometrics 1967;23:115–35. doi: 10.2307/2528285
- 414 [30] Ganas K, Divino JN, Gherard KE, Davis JP, Mouchlianitis F, Schultz ET. A reappraisal of  
415 reproduction in anadromous Alewives: Determinate versus indeterminate fecundity,  
416 batch size, and batch number. Trans Am Fish Soc 2015;144:1143–58. doi:  
417 10.1080/00028487.2015.1073620
- 418 [31] Hyle AR, McBride RS, Olney JE. Determinate versus indeterminate fecundity in American  
419 shad, an anadromous clupeid. Trans Am Fish Soc 2014;143:618–33. doi:  
420 10.1080/00028487.2013.862178

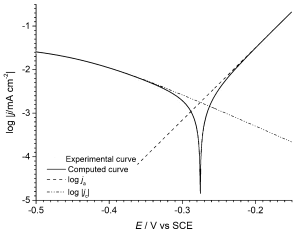
- 421 [32] R Core Team. R: A language and environment for statistical computing. R Foundation for  
422 Statistical Computing, Vienna, Austria; 2018. URL <https://www.R-project.org/>.
- 423 [33] Wickham H. Ggplot2: Elegant Graphics for Data Analysis. Springer-Verlag New York; 2016
- 424 [34] Wilke CO. Ggridges: Ridgeline Plots in 'ggplot2'. R package version 0.5.1.; 2018.  
425 <https://CRAN.R-project.org/package=ggridges>
- 426 [35] Kassambara A. Ggpubr: 'ggplot2' Based Publication Ready Plots. R package version 0.2.3.;  
427 2019. <https://CRAN.R-project.org/package=ggpubr>
- 428 [36] McMartin K, Jordaan A, Sclafani M, Cerrato R, Frisk MG. A new paradigm in Alewife  
429 migration: oscillations between spawning grounds and estuarine habitats. Trans Amer  
430 Fish Soc 2019;148(3):605–19. doi: 10.1002/tafs.10155
- 431 [37] Lowerre-Barbieri SK, Barbieri LR, Flanders JR, Woodward AG, Cotton CF, Knowlton MK.  
432 Use of passive acoustics to determine Red drum spawning in Georgia waters. Trans Amer  
433 Fish Soc 2008;137:562–75. doi: 10.1577/T04-226.1
- 434 [38] Murayama T, Shiraishi M, Aoki I. Changes in ovarian development and plasma levels of  
435 sex steroid hormones in the wild female Japanese sardine (*Sardinops melanostictus*)  
436 during the spawning period. J Fish Biol 1994;45(2):235–45. doi: 10.1111/j.1095-  
437 8649.1994.tb01303.x
- 438 [39] Bradford CS, Taylor MH. Semilunar changes in estradiol and cortisol coincident with  
439 gonadal maturation and spawning in the Killifish *Fundulus heteroclitus*. Gen Comp Endoc  
440 1987;66:71–8.
- 441 [40] Kobayashi M, Aida K, Hanyu I. Hormone changes during the ovulatory cycle in goldfish.  
442 Gen Comp Endoc 1988;69:301–7.
- 443 [41] Schaefer KM. Spawning time, frequency, and batch fecundity of yellowfin tuna, *Thunnus*  
444 *albacares*, near Clipperton Atoll in the eastern Pacific Ocean. Fish Bull 1996;94:98–112.
- 445 [42] Nyuji M, Takasuka A. Spawning cycle and fecundity of a multiple spawner round herring  
446 *Etrumeus teres* off southern Japan: Oocyte growth and maturation analysis. J Sea Res  
447 2017;122:11–8.
- 448 [43] Shirokova MY. Peculiarities of the sexual maturation of females of the Baltic cod, *Gadus*  
449 *morhua callarias*. J Ichthyol 1977;17(4):574–81.
- 450 [44] Grier HJ, Porak WF, Carroll J, Parenti LR. Oocyte development and staging in the Florida  
451 bass, *Micropterus floridanus* (LeSueur, 1822), with comments on the evolution of pelagic  
452 and demersal eggs in bony fishes. Copeia 2018;106:329–45.
- 453 [45] Witthames PR, Thorsen A, Murua H, Saborido-Rey F, Greenwood LN, Dominguez R, Korta  
454 M, Kjesbu OS. Advances in methods for determining fecundity: application of the new  
455 methods to some marine fishes. Fish Bull 2009;107(2):148–64
- 456 [46] Hunter JR, Leong R. The spawning energetics of female northern anchovy, *Engraulis*  
457 *mordax*. Fish Bull 1981;79:215–30.

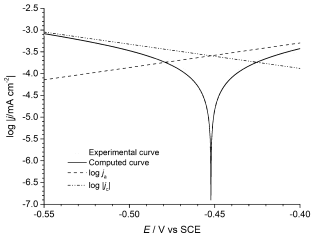
458 [47] Ganas K, Lowerre-Barbieri SK, Cooper W. Understanding the determinate –  
459 indeterminate fecundity dichotomy in fish populations using a temperature dependent  
460 oocyte growth model. J Sea Res 2015;96:1–10.

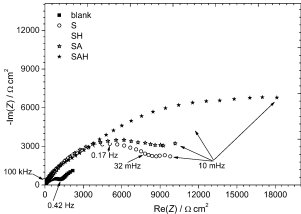




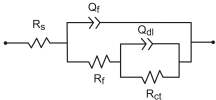








(a)



(b)

